Impact of Cloud Model Microphysics on Passive Microwave Retrievals of Cloud Properties. Part II: Uncertainty in Rain, Hydrometeor Structure, and Latent Heating Retrievals

EUN-KYOUNG SEO AND MICHAEL I. BIGGERSTAFF

School of Meteorology, University of Oklahoma, Norman, Oklahoma

(Manuscript received 11 August 2004, in final form 2 September 2005)

ABSTRACT

The impact of model microphysics on the retrieval of cloud properties based on passive microwave observations was examined using a three-dimensional, nonhydrostatic, adaptive-grid cloud model to simulate a mesoscale convective system over ocean. Two microphysical schemes, based on similar bulk two-class liquid and three-class ice parameterizations, were used to simulate storms with differing amounts of supercooled cloud water typical of both the tropical oceanic environment, in which there is little supercooled cloud water, and midlatitude continental environments in which supercooled cloud water is more plentiful. For convective surface-level rain rates, the uncertainty varied between 20% and 60% depending on which combination of passive and active microwave observations was used in the retrieval. The uncertainty in surface rain rate did not depend on the microphysical scheme or the parameter settings except for retrievals over stratiform regions based on 85-GHz brightness temperatures T_B alone or 85-GHz T_B and radar reflectivity combined. In contrast, systematic differences in the treatment of the production of cloud water, cloud ice, and snow between the parameterization schemes coupled with the low correlation between those properties and the passive microwave T_B examined here led to significant differences in the uncertainty in retrievals of those cloud properties and latent heating. The variability in uncertainty of hydrometeor structure and latent heating associated with the different microphysical parameterizations exceeded the inherent variability in T_B–cloud property relations. This was true at the finescales of the cloud model as well as at scales consistent with satellite footprints in which the inherent variability in T_B–cloud property relations are reduced by area averaging.

1. Introduction

Latent heating associated with tropical rainfall is known to be an important part of the global energy budget (e.g., Riehl and Malkus 1958; Malkus 1962; Riehl and Simpson 1979). Moreover, large-scale circulations have been shown to be sensitive to the vertical profile of diabatic heating (Hartmann et al. 1984; DeMaria 1985). The goal of the Tropical Rainfall Measuring Mission (TRMM) is to estimate rainfall and its vertical distribution of latent heating throughout the Tropics (Simpson et al. 1988; Kummerow et al. 2000).

To retrieve rain and latent heating, the TRMM satellite relies on observations from a passive microwave radiometer, the TRMM Microwave Imager (TMI), and a 13.8-GHz precipitation radar (PR) (Kummerow et al. 1998). Measurements from these instruments are used in conjunction with databases from cloud dynamical–microphysical and radiative transfer models to obtain rainfall and latent heating profiles that are consistent with the satellite observations (e.g., Kummerow et al. 1996; Olson et al. 1996, 1999).

The accuracy of the retrieved cloud properties depends, in part, on how representative the model manifold of passive microwave brightness temperatures T_B are of the T_B relations in naturally occurring storms (Panegrossi et al. 1998). Panegrossi et al. (1998) emphasized the affect of environmental characteristics on the manifolds (multidimensional relations) of simulated passive microwave T_B and also suggested that model microphysical parameterizations could affect the T_B manifold.

To examine the sensitivity of T_B–cloud property relations on model microphysics, Biggerstaff et al. (2006, hereinafter Part I) used a set of numerical simulations

Corresponding author address: Dr. Michael I. Biggerstaff, School of Meteorology, University of Oklahoma, 100 E. Boyd Street, SEC Rm. 1310, Norman, OK 73019.
E-mail: drdoppler@ou.edu

© 2006 American Meteorological Society

of a squall line taken from Hristova-Veleva (2000). She tuned two microphysical schemes, each based on a three-class ice and two-class water bulk parameterization method, to generate storms that were consistent with both a tropical oceanic regime in which accumulations of supercooled cloud water are low and a midlatitude continental regime in which accumulations of supercooled cloud water are more plentiful. This goal was accomplished by adjusting the initial number of ice crystals that were assumed to be activated at 0°C (the so-called NCIO parameter). A low NCIO value allowed supercooled cloud water to accumulate. A high NCIO setting ensured that enough cloud ice was generated to use the available excess water vapor effectively, leading to low concentrations of supercooled cloud water.

In their numerical simulations, Adler et al. (1991) found that supercooled cloud water masked the scattering of high-frequency microwave energy by graupel by absorbing the scattered energy and reemitting it. This effect for the simulations conducted by Hristova-Veleva (2000) was calculated in Part I, and, on average, a warming of 15 K in 85-GHz T_B over the convective region of the low-NCIO simulations was found. This effect was sufficient to shift the model T_B manifolds and produce variability in the relations between cloud properties and passive microwave T_B at TMI frequencies. Moreover, in Part I it was shown that this effect depended on which parameterization scheme was used in the cloud model. This result led to the conclusion that retrievals of latent heating and hydrometeor profiles are sensitive to model microphysical parameterizations.

This study further quantifies the uncertainty of retrieved cloud properties and its sensitivity to model microphysics. We made use of the empirical orthogonal function (EOF) framework developed in Part I to examine systematic differences in retrievals of cloud properties associated with changes in the model microphysics. To test the significance of these findings, we compared the variability associated with the different microphysical schemes with the inherent variability between cloud properties and small changes in microwave brightness temperatures. For the parameter space examined here, it was found that one microphysical scheme exhibited differences in hydrometeor and latent heating profile structure that significantly exceeded the inherent variability in the T_B–cloud property relations. The other scheme did not. This was true at the finescales of the cloud model as well as at scales typical of satellite footprints for which the inherent variability in T_B–cloud property relations is reduced by area averaging.

The results presented here suggest that, depending on which microphysical parameterization is used in the model, the impact of model microphysics on retrieved hydrometeor and latent heating structure over satellite-footprint scales can exceed the inherent uncertainty associated with nonuniqueness in T_B–cloud property relations. When considering the surface rain rate by itself, however, the inherent variability in T_B–rain rate relations was significantly greater than the variability among the four microphysical parameterizations.

2. Data sources

a. Models in use

The data for this study were taken from simulations of a mesoscale convective system conducted by Hristova-Veleva (2000) and are described in Part I. The microphysical parameterization schemes used in the model are variants of Lin et al. (1983), taken from Tao and Simpson (1993), and of Rutledge and Hobbs (1984), taken from Keenan et al. (1994). These bulk microphysical schemes employ parameterizations for two classes of liquid water (cloud water and rain) and three classes of ice (cloud ice, snow, and graupel).

Here we make use of the four simulations that have temperature-independent collection efficiencies for graupel collecting snow and snow collecting cloud ice. They are referred to as AM_eH_i, AM_eL_i, BM_eH_i, and BM_eL_i, where the first character indicates the particular variant of the parameterization scheme [A for those based on a graupel version of Tao and Simpson (1993) and B for those based on the scheme used in Keenan et al. (1994)]. The second character, with subscript "e," refers to the temperature-independent collection efficiencies that were set equal in all four simulations used here. The third character, with subscript "i," denotes the value of the assumed number of activated ice crystals at 0°C (the NCIO parameter), with L_i representing a value of 10^{-2} m^{-3} and H_i representing values greater than 10^7 m^{-3}. As discussed in Part I, the first value was chosen to represent environments that support accumulation of supercooled cloud water, like midlatitudes with high concentrations of cloud condensation nuclei, where cloud water is distributed over a large number of small particles that can be carried aloft in the convective updrafts. The latter value was set artificially high to ensure that the condensed water vapor would be assigned to cloud ice rather than to cloud water in the simulation. This approach was done to represent environments that produce clouds with little supercooled cloud water, like tropical oceanic regimes and the Amazon (e.g., Stith et al. 2002). Hence, the comparisons of AM_eH_i (BM_eH_i) versus AM_eL_i (BM_eL_i) allow for examination of the impact of supercooled cloud water on

relationships between brightness temperatures and cloud properties. In a similar way, the comparisons of AM_eH_i (AM_eL_i) versus BM_eH_i (BM_eL_i) allow for examination of the sensitivity of the results to a particular implementation of the microphysical parameterizations.

Microwave brightness temperatures were calculated from the hydrometeor profiles produced in the cloud model using a one-dimensional Eddington's second-approximation radiative transfer model (Weinman and Davies 1978; Kummerow 1993), as described in Part I. Brightness temperatures are calculated at 10, 19, 21, 37, and 85 GHz, the same as the TMI channels, with nadir viewing assumed for simplicity.

b. Simulations and model data

All model-generated variables, including microphysical mass contents in a unit volume (densities), latent heat release, and vertical velocity, were archived. The model output during the mature stage (Leary and Houze 1979) of the simulated storm was sampled at 6×6 km^2 horizontal resolution and 700-m vertical resolution with a temporal resolution of 5 min. All precipitation points in the dataset were classified as either convective or stratiform following the procedure of Tao and Simpson (1993). About 10 000 vertical profiles were taken through each convective and stratiform cloud during the mature stage of each simulated storm system to create the database used here.

3. Method

a. EOF framework

Passive microwave brightness temperatures associated with upwelling emission from the earth's surface are a function of hydrometeor content, surface emissivity and temperature, and atmospheric constituents and temperature. Surface emissivity and precipitation-sized hydrometeors are crucial in determining T_B at TMI frequencies. The other terms are negligible (e.g., Kummerow et al. 1991; Smith et al. 1992; Heymsfield and Fulton 1988). Assuming a fairly uniform surface emissivity, T_B can be expressed as a function of the vertical distribution and content of hydrometeors. As shown by Part I, within about 80% of total variance, the vertical profiles of hydrometeors in the model can be expressed in terms of their first EOF and its coefficient. Thus, T_B can be expressed as

$$T_B \cong f(\bar{\mathbf{h}}_c + a_c\hat{\mathbf{e}}_c, \bar{\mathbf{h}}_r + a_r\hat{\mathbf{e}}_r, \bar{\mathbf{h}}_i + a_i\hat{\mathbf{e}}_i, \bar{\mathbf{h}}_s + a_s\hat{\mathbf{e}}_s, \bar{\mathbf{h}}_g + a_g\hat{\mathbf{e}}_g), \tag{1}$$

where $\bar{\mathbf{h}}_j$, a_j, and $\hat{\mathbf{e}}_j$ denote the mean vertical profile, the EOF coefficient (or amplitude), and the EOF, respectively, of the jth hydrometeor. The subscripts c, r, i, s, and g denote cloud water, rain, cloud ice, snow, and graupel, respectively.

The quantities $\bar{\mathbf{h}}_j$ and $\hat{\mathbf{e}}_j$ are constant vectors determined from one of the four simulations. Note that information regarding the vertical structure of hydrometeors is contained in a zero-dimensional parameter, the EOF coefficient. Hence, the only variables in (1) are the coefficients a_j. As a consequence, (1) can be expressed in terms of the EOF coefficients:

$$T_B \cong g(a_c, a_r, a_i, a_s, a_g). \tag{2}$$

Equation (2) implies that a brightness temperature can be determined from a combination of only the first EOF coefficients of individual hydrometeor profiles. The inverse is also true. The first EOF coefficient of a hydrometeor can be determined from a set of brightness temperatures. This approximation is generally good over uniform or weakly varying surface emissivities when the first eigenvalue represents most of the variance in the vertical structure of the hydrometeor profiles.

The first EOF coefficient of a cloud model variable based on (2) can be retrieved from a set of T_B at TMI frequencies using multivariate linear regression:

$$\tilde{a}_j = b_0 + b_1T_1 + b_2T_2 + b_3T_3 + b_4T_4 + b_5T_5(+b_6a_{\text{ref}}), \tag{3}$$

where $\tilde{a}_j$ is the retrieved EOF coefficient of the jth hydrometeor, T_i represents the T_B at the ith microwave frequency, b_i is the regression coefficient associated with the ith predictor (e.g., the ith T_B frequency), and a_{ref} denotes the first EOF coefficient of radar reflectivity from the model database that can be used as an additional predictor to evaluate the benefit of the PR data available on the TRMM satellite relative to just the TMI data.

Because there is a strong relationship between the vertical structure of hydrometeors and radar reflectivity, latent heating, and vertical motion, the T_B can also be used to retrieve the first EOF coefficient of those model variables. It is obvious that, for the analysis conducted here, inclusion of a_{ref} in (3) should lead to a perfect result when retrieving the EOF coefficient of radar reflectivity.

Although the microwave T_B and the EOF coefficient of radar reflectivity are used to retrieve a scalar quantity, the EOF coefficient, a vertical profile of that variable at an individual column can be reconstructed. The reconstructed profile is the mean profile of that variable from the model database added to the product of the retrieved EOF coefficient and the first EOF of that

variable. Hence, the vertical structure of hydrometeors or reflectivity, latent heating, and vertical motion that is consistent with a set of observed T_B at a given point in space can be retrieved using (3).

b. Coefficients of determination

Uncertainty in the multivariate linear regression can be estimated based on the regression's coefficient of determination (Neter et al. 1996), which represents a proportionate reduction of total variation associated with the predictor variables. The coefficient of determination R_j^2 associated with retrieving the jth variable is given by

$$R_j^2 = \sum_i (\tilde{a}_i - \bar{a})^2 \Big/ \sum_i (a_i - \bar{a})^2, \tag{4}$$

where $\tilde{a}$ is the retrieved EOF coefficient, $\bar{a}$ is the mean EOF coefficient for that variable in the model database, and a_i is the true value of the EOF coefficient at the ith point in the database. Because R_j^2 represents the amount of variance explained by the multivariate linear regression model, the uncertainty associated with this retrieval can be defined as

$$U_{\tilde{a}_j} = 1 - R_j^2. \tag{5}$$

4. Results

a. Uncertainty in retrieving EOF coefficients of cloud properties

Figure 1 shows the coefficients of determination associated with retrievals of surface rainfall rate and the first EOF coefficient for hydrometeor species, radar reflectivity, vertical motion, and latent heating using the most independent TMI channels (10 and 85 GHz) separately, all TMI channels combined, 85 GHz plus the profiles of radar reflectivity, and all TMI channels plus the profiles of radar reflectivity. These choices were made to illustrate the potential benefits of complementary passive and active microwave data sources and to provide insight to application over land where only the 85-GHz channel provides useful information because of the high, inhomogeneous surface emissivity (cf. Kummerow et al. 2000).

1) SURFACE RAIN RATE

The primary goal of TRMM is to measure tropical rainfall. In the model, surface precipitation rate (Pr) is calculated from the rain mass at the lowest level combined with the computed fall speeds and vertical motion of the air at that point. The set of T_B associated with the surface rain rate is computed from the entire hydrometeor profile. Retrieval of surface rain rate is performed directly from the multivariate linear regression using brightness temperatures. This is independent from the retrieval of the EOF coefficient of the rain profile. Both rain quantities are represented in Fig. 1.

(i) Convective region surface rain rate

All four simulations show that the uncertainty in retrieving surface rain rate over convective areas varies between 20% and 60% depending on the type of information used in the multivariate linear regression. The uncertainty in retrieved surface rain rate over the convective region did not depend on the microphysical scheme or the parameter settings tested here. As expected, the lowest uncertainty in surface rain rate was achieved using all of the available passive and active microwave information. However, there was little difference between having all of the information and using just the 10-GHz channel.

The greatest uncertainty occurred when the retrieval was limited to just the 85-GHz channel. This result is consistent with Part I in which it was noted that the impact of microphysical parameterizations was most evident when the rain profiles were sorted by 85-GHz T_B alone. The addition of radar reflectivity to 85-GHz T_B added skill to the retrieval but was still about 20% more uncertain than using the combined TMI channels. This result implies that retrievals over land, even with reflectivity from the PR, will be considerably more uncertain than retrievals over water for which the lower-frequency channels are able to contribute information on the underlying cloud structures.

(ii) Stratiform region

In contrast to convective regions, where the retrieval of surface rain rate was independent of the microphysical parameterization scheme, the retrieval of surface rain rate over stratiform regions showed considerable variation among simulations. This variation was almost entirely due to an overall reduction in the coefficient of determination associated with retrievals using 85-GHz T_B by itself, or 85 GHz and radar reflectivity combined, in the low-ice runs. This result is due to the influence of snow on the surface rain rate in the stratiform region. Snow accounts for about 30% of the surface rain rate in the simulated stratiform regions and less than 10% in the simulated convective regions. Both parameterization schemes had lower correlations between snow and 85-GHz T_B in the low-ice runs than in the high-ice runs, with scheme B exhibiting the lowest correlation (Part I). Hence, 85-GHz T_B by itself is not sufficient for retrieving surface rain rate in the stratiform region, espe-

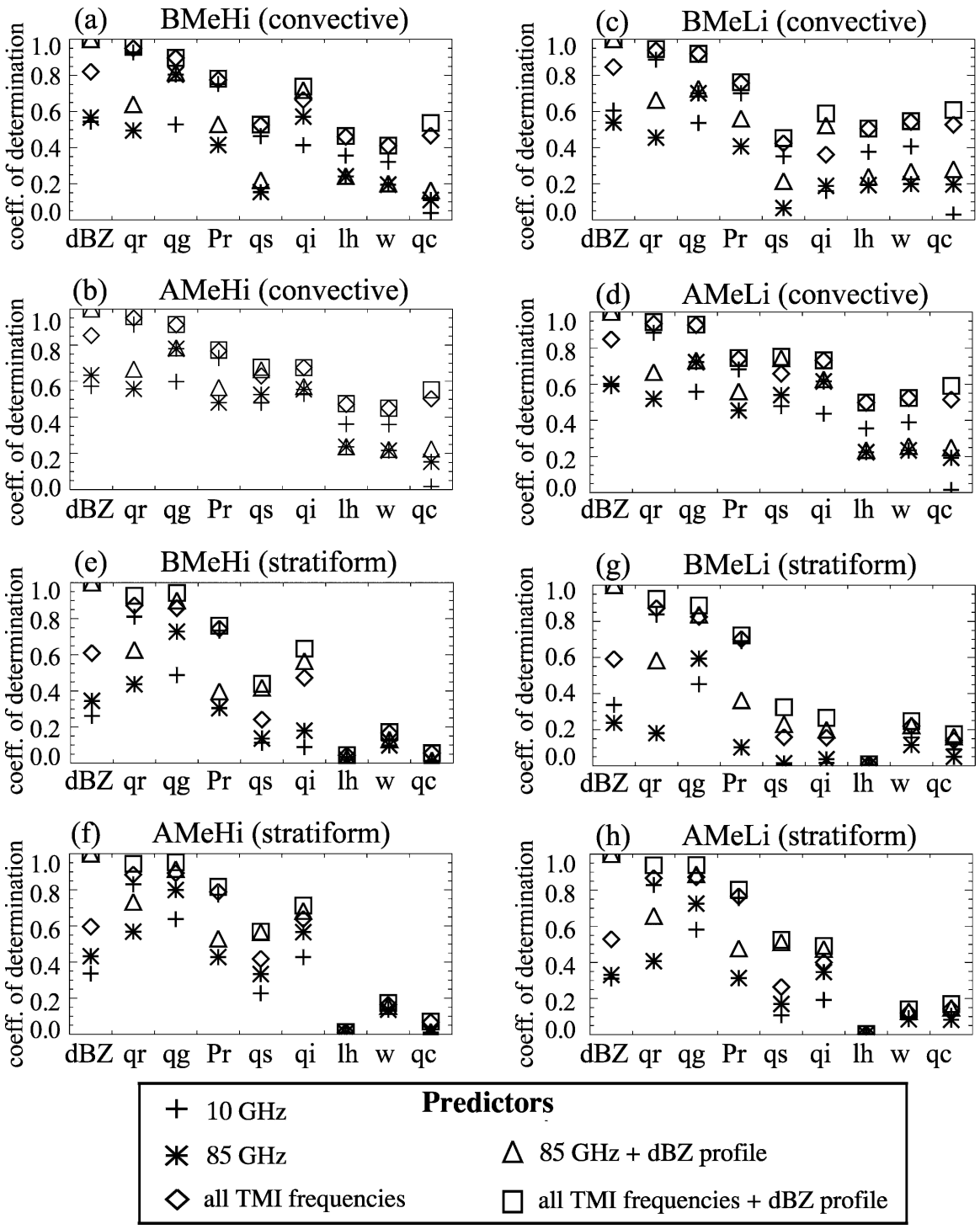

FIG. 1. The coefficients of determination for the first EOF coefficients of vertical profiles of model variables using the predictors indicated in the legend for the (a) BM_eH_i convective, (b) AM_eH_i convective, (c) BM_eL_i convective, (d) AM_eL_i convective, (e) BM_eH_i stratiform, (f) AM_eH_i stratiform, (g) BM_eL_i stratiform, and (h) AM_eL_i stratiform regions. The axis labels dB*Z*, qr, qg, Pr, qs, qi, lh, w, and qc refer to radar reflectivity, rain, graupel, surface precipitation rate, snow, cloud ice, latent heating, vertical motion, and cloud water, respectively.

cially for scheme B. Because radar reflectivity is affected by snow, inclusion of reflectivity in the retrieval had a measurable positive impact.

When the retrieval of surface rain rate is able to include 10-GHz T_B, variability in the uncertainty of surface rain rate no longer depends significantly on the model microphysical parameterizations for the settings examined here at high spatial resolution.

(iii) Rain profile versus surface rain rate

As noted by Smith et al. (1992), passive microwave observations are better correlated with vertically integrated hydrometeor mass than with surface precipitation rate. In Part I it was shown that the magnitude of the EOF coefficient may be used as a proxy for integrated hydrometeor mass while preserving the vertical structure of the hydrometeor profile. In agreement with Smith et al. (1992), the coefficient for determination for the first EOF coefficient of the rain profile (Fig. 1) is higher than the coefficient of determination for the surface rain rate. Indeed, using 10-GHz T_B, or any combination of passive and active microwave observations with 10-GHz T_B, led to an uncertainty in the retrieved EOF coefficient of less than 10% over both convective and stratiform regions. Based on the modeling work analyzed here, the uncertainty in surface rain rate is about 4 (2) times the uncertainty in retrieving the first EOF coefficient of the rainwater profile over convective (stratiform) regions.

2) OTHER PRECIPITATION-SIZED HYDROMETEORS

Like rain, retrieval of the first EOF coefficient for graupel over both convective and stratiform regions has fairly low uncertainty when all the passive and active microwave information is used (Fig. 1). However, the graupel retrieval benefits more from the full range of TMI channels. There is between 10% and 20% further reduction in uncertainty using the full suite of TMI frequencies relative to using the single best channel—85 GHz in this case. The improvement is greater for the low-ice simulations in which supercooled cloud water masks the 85-GHz T_B scattering signature. In that regard, model microphysical parameterizations have an effect on the uncertainty in the retrieved EOF coefficients of graupel.

Retrievals of the EOF coefficient for snow (Fig. 1) have significant uncertainty, 30%–60% in the convective region and 50%–80% in the stratiform region. Differences in the microphysical parameterizations are clearly evident, with scheme B showing the greatest uncertainty in the retrieval. As noted in Hristova-Veleva (2000), scheme A tended to have a vertically layered hydrometeor structure in which higher concentrations of snow corresponded to higher concentrations of graupel and rain. Scheme B had a more uniform distribution of snow and cloud ice. TMI frequencies are more sensitive to graupel and rain than snow (Part I). Thus, in simulations using scheme A, the uncertainty in retrieval of EOF coefficients for snow was reduced by the strong correlations between mass contents of the precipitation-sized particles. This result is particularly well illustrated by the behavior of retrievals over convective regions based on 85-GHz T_B. In scheme B, 85-GHz T_B was a poor predictor of snow, even when combined with radar reflectivity. In contrast, for scheme A, 85-GHz T_B was a moderately good predictor or snow, even when used by itself.

In naturally occurring leading-line trailing-stratiform squall line systems, the stratiform region is often dominated by snow and very little graupel exists (e.g., Willis and Heymsfield 1989). Given the weak influence of snow on TMI brightness temperatures, the uncertainty in retrieving snow in natural cloud systems is likely greater than the results indicated here.

3) CLOUD PARTICLES

Similar to snow, the uncertainty in retrieving the EOF coefficient of cloud ice and cloud water depended strongly on the microphysical parameterization used in the cloud model and on whether the clouds were convective or stratiform (Fig. 1). Of the hydrometeor fields, retrieval of cloud water showed the greatest benefit to including the full suite of TMI channels. This situation is due to the positive correlation between cloud water and 37-GHz T_B in the convective region (Part I). The 37-GHz channel is affected by both emission and scattering. Although warming of T_B at 37 GHz through emission from liquid water is quickly saturated in the presence of rain, the simulated convective region contained many developing clouds that had high cloud water content but little rain. Thus, in convective regions where cloud water contents are sufficiently high and rain content is sufficiently low, retrievals of the EOF coefficient for cloud water are less uncertain (50%) than in stratiform regions (~90%) where cloud water concentrations are simply too low.

4) VERTICAL MOTION AND LATENT HEATING

Passive microwave retrievals of latent heating from a cloud model database represent the instantaneous heating associated with the phase changes of water over the scale of the brightness temperature observation. Shige et al. (2004) note that the average of the retrieved instantaneous latent heating profiles can be interpreted

as the mean large-scale latent heating associated with the apparent heat source from the convective system (Yanai et al. 1973; Johnson 1984) as long as the cloud-resolving model adequately reproduces the life cycle and statistics of the precipitation of the observed storm. Here we are interested in differences in the retrievals that arise from microphysical parameterizations that affect the statistical representation of the precipitation in the cloud model.

Retrievals of the EOF coefficients of cloud properties that are indirectly related to hydrometeor profiles, such as vertical motion and latent heating (Fig. 1), illustrate differences in the fundamental nature of convective and stratiform precipitation. In convective regions, microphysical processes are dominated by local effects associated with small-scale vertical motions that have magnitudes similar to or greater than the horizontal flow. Thus, the vertical profile of latent heating and vertical motion over the convective region should be strongly related to the vertical profile of hydrometeors.

In contrast, microphysical processes in stratiform regions are driven by advection of particles and momentum from the convective region (Rutledge and Houze 1987; Biggerstaff and Listemaa 2000). Latent heating in stratiform clouds depends more on easily advected hydrometeors such as cloud water, cloud ice, and low-density snow than does latent heating in convective clouds (Tao et al. 1990). Moreover, vertical motion is considerably weaker than horizontal motion in stratiform clouds. Hence, growth of precipitation particles and the associated release of latent heating occur over a more horizontal trajectory in stratiform regions. As a consequence, there is less connection between the vertical profile of hydrometeors and vertical motion and latent heating in stratiform clouds. This situation is clearly illustrated by the near-zero coefficient of determination for latent heating and vertical motion in stratiform regions as compared with the moderate values of the coefficient of determination in convective regions of the four simulations (Fig. 1).

It should be understood that the uncertainty in retrieving the EOF coefficient is not the same as the uncertainty in retrieving the profile of a model variable. For stratiform-region latent heating, the results simply imply that the retrieval based on passive microwave information at TMI frequencies cannot be improved beyond knowing the mean profile.

b. Inherent variability in T_B–cloud property relations

To test whether differences in microphysical parameterizations are a significant source of uncertainty in retrievals of hydrometeor and latent heating profiles, it is necessary to examine the magnitude of those differences relative to the inherent variability in T_B–cloud property relations.

1) Examples of variability near a given T_B vector

(i) Definition of parameters

If we let a target T_B vector $\mathbf{T}_j$ associated with an individual hydrometeor profile have components corresponding to T_B of 10, 19, 21, 37, and 85 GHz, then we can define a difference ΔT between the target vector and another T_B vector $\mathbf{T}_k$ associated with a different hydrometeor profile within the database as

$$\Delta T = |\mathbf{T}_j - \mathbf{T}_k|. \tag{6}$$

The variability in T_B–cloud property profiles can be examined by plotting individual profiles from the model database that are within a few kelvins from the target vector (Fig. 2). It is important to note that the profiles in Fig. 2 were taken directly from a search through the model database and were not reconstructed from an EOF retrieval.

To quantify differences between vertical profiles, a structural difference parameter is defined. If we let $\mathbf{q}_j$ be the column vector associated with the reference vertical profile of some model variable, then the structural difference between the reference and another profile $\mathbf{q}_k$ can be expressed as

$$\Delta q = |\mathbf{q}_j - \mathbf{q}_k|/|\mathbf{q}_j| \times 100. \tag{7}$$

To aid interpretation of the structural difference between two column vectors, several examples from idealized profiles are provided in Fig. 3.

(ii) Cloud particles and snow

Even in the same simulation, there exist fluctuations in the vertical structures of hydrometeors for small changes from a given set of T_B (Fig. 2). Consistent with their lack of influence on and low correlation with TMI T_B, cloud water, cloud ice, and snow exhibited a high degree of variability. The structural differences in these parameters also depended significantly on the particular microphysical scheme used in the cloud model, with profiles from scheme-B simulations having more variability than profiles from scheme-A simulations. Variability in cloud ice and cloud water for a given set of T_B also depended strongly on the choice of NCIO within each parameterization scheme.

(iii) High-density precipitation particles and radar reflectivity

Profiles of rain and graupel, which are strongly correlated with T_B at TMI frequencies, exhibited consid-

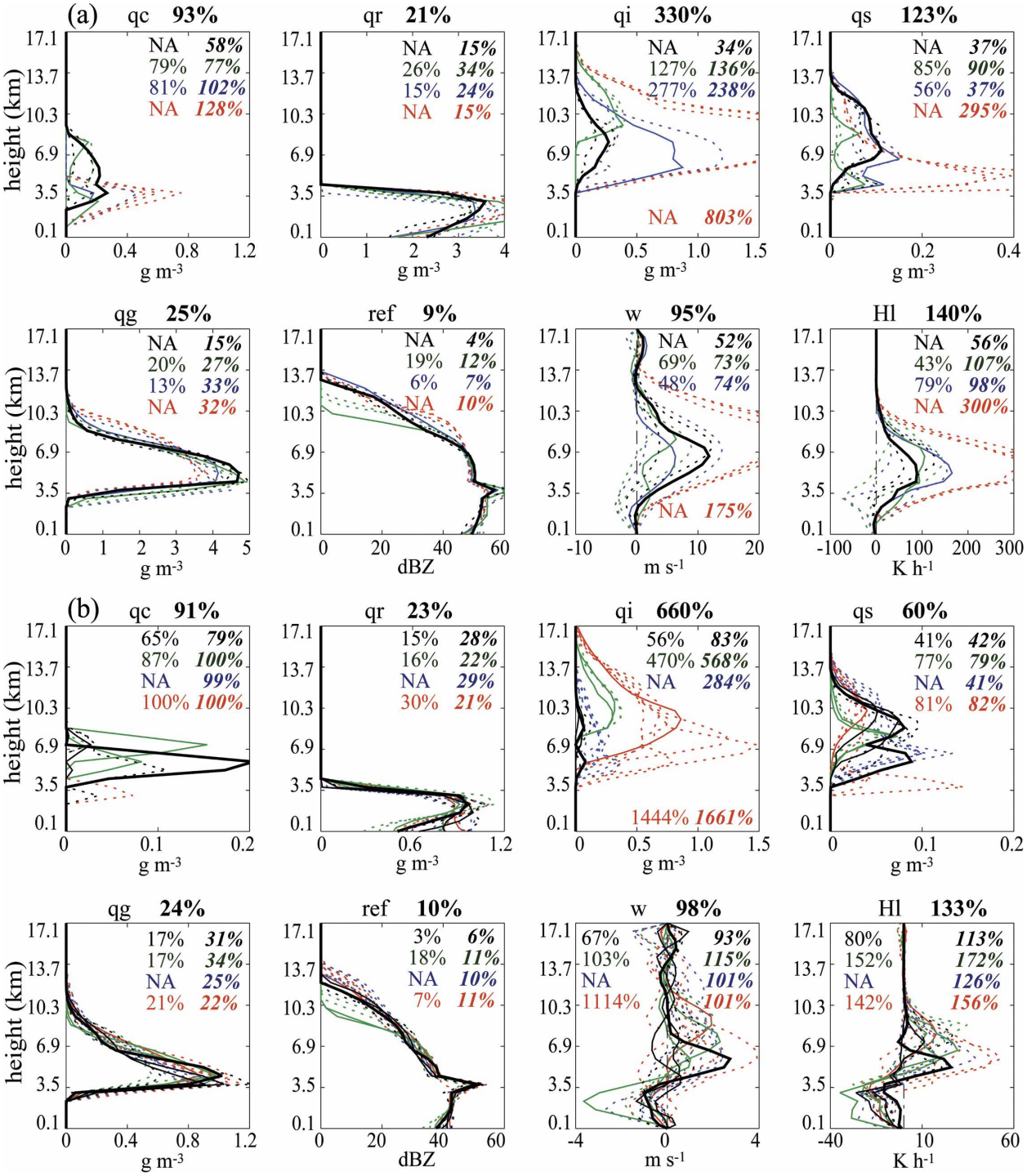

FIG. 2. Vertical profiles of microphysical variables whose T_B vectors for the four microphysical schemes are within 3 (solid lines) or 3–6 (dotted lines) K from target T_B vectors from AM_eL_i of (a) T_B = (260.8, 216.1, 200.1, 132.8, 121.1 K) for a convective profile and (b) T_B = (177.3, 248.1, 257.3, 241.8, 197.0 K) for a stratiform profile. The panel labels qc, qr, qi, qs, qg, ref, w, and Hl denote cloud water, rain, cloud ice, snow, graupel, radar reflectivity, vertical velocity, and latent heat release, respectively. Black, green, blue, and red lines denote AM_eL_i, BM_eL_i, AM_eH_i, and BM_eH_i, respectively. Black solid lines denote the vertical profiles of microphysical variables corresponding to the target vectors. Regular and boldface italic fonts inside panels denote averaged structural differences in percent for ΔT within 3 (solid lines) and 3–6 (dotted lines) K, respectively; "NA" indicates that no data point existed within a particular model database for that range of ΔT. The averaged structural differences within ΔT of 4 K for all microphysical schemes are shown above the panels.

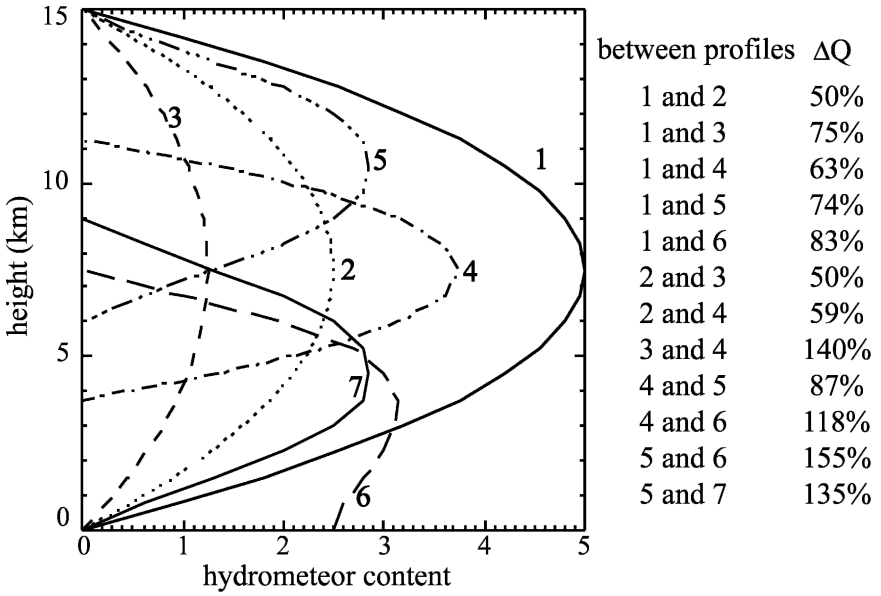

FIG. 3. Structural differences (ΔQ) between selected idealized profiles. Note that the largest structural differences occur for vertical displacements as opposed to differences in magnitude between the profiles.

erably less variation across the four simulations than did the profiles of cloud ice, cloud water, or snow. Nevertheless, for both convective and stratiform clouds, near-surface rainwater content varied by a factor of 2 with little impact on the brightness temperature vector.

The dichotomy in T_B–hydrometeor relations between high-density and low-density precipitation particles contributed to strong variability in the upper-level radar reflectivity profiles associated with small changes in **T**. At altitudes above 10 km, where snow dominates the reflectivity, differences on the order of 20–30 dB were found. In contrast, at lower altitudes where rain and graupel dominate reflectivity, the profiles were within a few decibels of each other.

(iv) Latent heating and vertical motion

There were tremendous fluctuations in latent heating profiles in the model database for just a few degrees of change in the input brightness temperature vector, even within the same microphysical scheme. Indeed, over the convective region where latent heating was moderately correlated to T_B at TMI frequencies, the profiles of latent heating varied from strong "convective like" (Houze 1982) structures to strong "stratiform like" structures.

The magnitude of the variability also depended on the microphysical parameterizations used in the model, with scheme-B simulations exhibiting more variability than did scheme-A simulations. Profiles that exhibited significantly higher cloud ice concentrations typically had stronger latent heating at midlevels (red dotted lines in Fig. 2a). Moreover, the simulations in which the peak cloud ice concentrations were found at higher altitudes (BM_eL_i) also had latent heating maxima at higher altitude than did the latent heating profiles associated with the target **T**.

Similar to latent heating, vertical velocity profiles show a large degree of variability for small changes in **T**. This is particularly true for the convective region, for which vertical motions at mid- to upper levels varied from 2 to more than 20 m s^{-1} within a target set of T_B.

2) GENERATING STRUCTURAL DIFFERENCES FOR A MODEL DATABASE

(i) Definition of parameters

To generalize the nonuniqueness in T_B–cloud property relations, the structural difference parameter is redefined to take into account all of the hydrometeors simultaneously. A column vector **Q**, containing all hydrometeor contents, is defined as

$$\mathbf{Q} = \begin{bmatrix} \alpha_c \mathbf{q}_c \\ \alpha_r \mathbf{q}_r \\ \alpha_i \mathbf{q}_i \\ \alpha_s \mathbf{q}_s \\ \alpha_g \mathbf{q}_g \end{bmatrix}, \tag{8}$$

TABLE 1. Average of correlations between TMI T_B and the first EOF coefficients of each hydrometeor species. Each row represents a microphysical scheme. Regular and italic fonts represent convective and stratiform clouds, respectively.

Correlation	Cloud water		Rain		Cloud ice		Snow		Graupel	
BM_eH_i	0.37	*0.03*	0.70	*0.84*	0.50	*0.32*	0.47	*0.37*	0.57	*0.73*
AM_eH_i	0.34	*0.03*	0.64	*0.87*	0.50	*0.68*	0.53	*0.51*	0.55	*0.82*
BM_eL_i	0.35	*0.33*	0.58	*0.84*	0.46	*0.48*	0.49	*0.36*	0.51	*0.78*
AM_eL_i	0.40	*0.30*	0.58	*0.81*	0.34	*0.14*	0.33	*0.09*	0.49	*0.70*

where $\mathbf{q}_j$ is a column vector representing a vertical profile of the jth hydrometeor species. The subscripts c, r, i, s, and g represent cloud water, rain, cloud ice, snow, and graupel, respectively. The coefficient α_j is a weight based on the average of the correlations between T_B at TMI channels and the first EOF coefficients of the jth hydrometeor species determined from the four simulations examined by Part I. The weighting factors are given in Table 1.

Because each TMI channel is not equally sensitive to individual hydrometeor species, the average-correlation weighting treats the definition of vertical structure of hydrometeor species more appropriately than does uniform weighting for all of the hydrometeor species. Thus, the definition given by (8) takes into account how well the TMI channels detect the individual hydrometeor species. More weight is given to rain than to the other hydrometeor species.

Generalizing the structural difference definition given in Kummerow and Giglio (1994), the structural difference in hydrometeor profiles (ΔQ), in percent, between two different column vectors can be defined as

$$\Delta Q = |\mathbf{Q}_j - \mathbf{Q}_k|/|\mathbf{Q}_j| \times 100, \quad (9)$$

where the subscripts j and k represent a reference vector and a compared vector, respectively. In a similar way, the structural difference in latent heating profiles is

$$\Delta H = |\mathbf{h}_j - \mathbf{h}_k|/|\mathbf{h}_j| \times 100, \quad (10)$$

where $\mathbf{h}$ represents a column vector for a latent heating profile. The structural difference for radar reflectivity profiles is

$$\Delta Z = |\mathbf{z}_j - \mathbf{z}_k|/|\mathbf{z}_j| \times 100, \quad (11)$$

where $\mathbf{z}$ represents a column vector for a vertical profile of radar reflectivity. The difference in surface precipitation rates is defined as

$$\Delta P = (p_j - p_k)/p_j \times 100, \quad (12)$$

where p represents a surface rain rate. All of the differences in hydrometeor structure, radar reflectivity, latent heating, and surface rain rate were sorted by the magnitude of the difference in the input T_B vector.

Based on the above definitions, the differences have been computed between all possible pairs in both convective and stratiform precipitation for the AM_eL_i simulation. This simulation was chosen as a reference because it exhibited characteristics consistent with the other three simulations and represented the middle of the range of variability found in the four simulations. The results were further divided by surface rain rate higher than 10 mm h^{-1} in convective clouds and 1 mm h^{-1} in stratiform clouds. Limiting the convective region to just the heavy precipitation cores allows for more direct interpretation of the statistical analysis. For convective clouds, there were about 11 million pairs available from the AM_eL_i simulation. For stratiform clouds, there were about 6.6 million pairs available.

(ii) Hydrometeor structure and surface precipitation rate

In taking into account all of the hydrometeors simultaneously, the average structural difference over convective cores increased quickly for the first few degrees of change in input T_B before logarithmically approaching 45% at ΔT of 20 K (Fig. 4). In the stratiform region the average structural difference increased more linearly with increasing ΔT. In general, the variability of the hydrometeor structure for the stratiform region was greater than that for the convective cores.

To appreciate better the variability in individual hydrometeor profiles that are consistent with the average structural differences shown in Fig. 4, we note that the average structural difference for the target vector used in Fig. 2a was 25% at ΔT of 3 K, using all of the profiles from the four simulations. The hydrometeor weighting based on the correlations with TMI frequencies minimized the impact of the cloud ice and snow, which had larger individual structural differences. The value of 25% at ΔT of 3 K agrees well with the overall mean structural difference of about 20% in the convective cores at ΔT of 3 K (Fig. 4a). Hence, weighted-average structural differences on the order of a few tens of percent correspond to relatively large variability in the structure of individual hydrometeor profiles.

The average variability of the surface rain rate was about 25% for a few degrees in ΔT over the convective

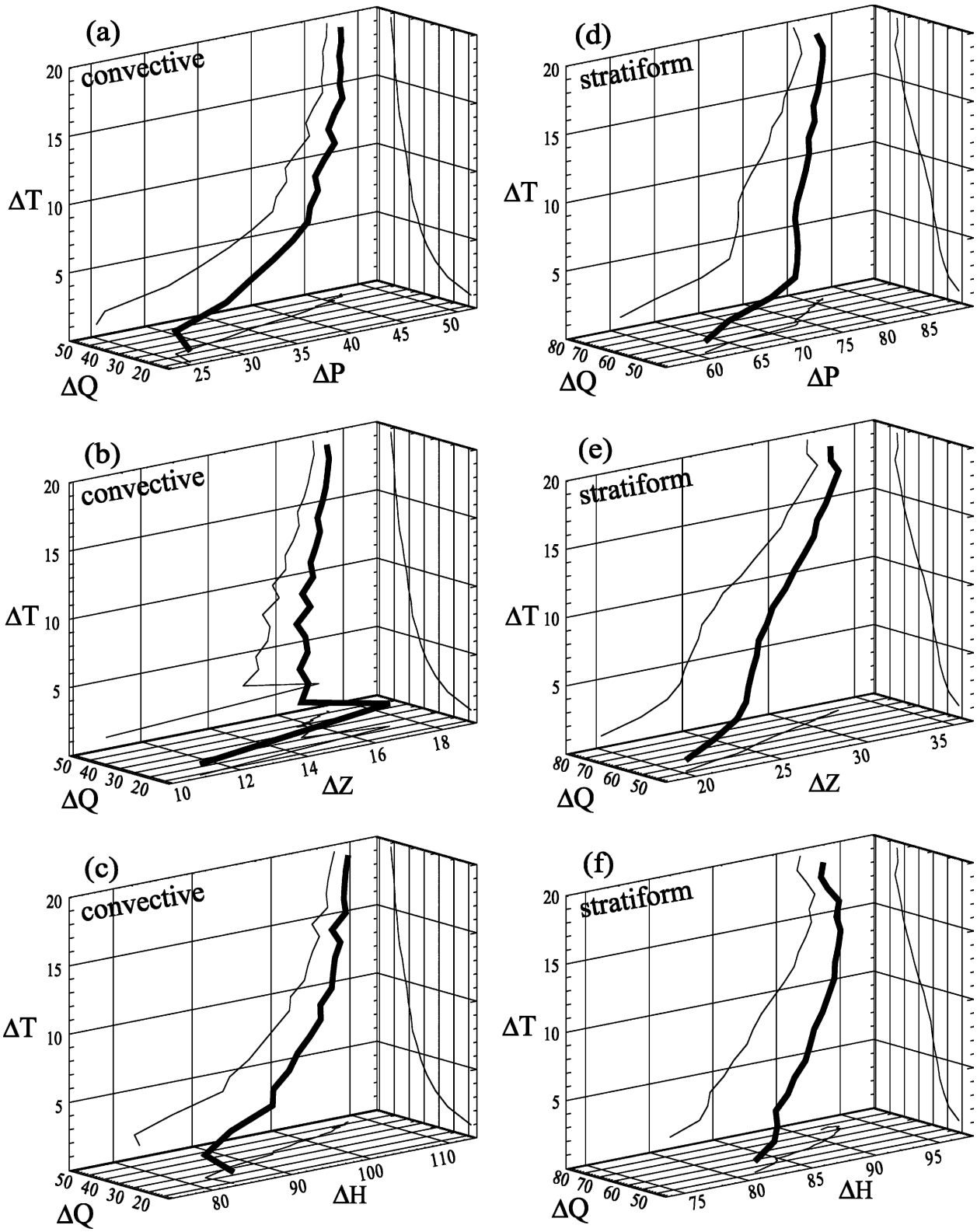

FIG. 4. Relationship between hydrometeor structure ΔQ (%) or input brightness temperature vector ΔT (K) and (a), (d) surface rain rate ΔP (%) or (b), (e) radar reflectivity ΔZ (%) or (c), (f) latent heating ΔH (%) for surface precipitation rates (left) higher than 10 mm h^{-1} in convective clouds and (right) higher than 1 mm h^{-1} in stratiform clouds.

cores and increased logarithmically with increasing ΔT, reaching a plateau of about 47% at 20 K. A similar variation was found for stratiform surface rain rate, but the uncertainty was greater by roughly a factor of 2.

(iii) Reflectivity and latent heating

The change in radar reflectivity structure is much smaller than changes in either the hydrometeor structure ΔQ or the surface rain rate ΔP for a given ΔT. Reflectivity is an integrated quantity that is weighted more by high-density precipitation-sized hydrometeors than by low-density small particles. Because the TMI frequencies are strongly correlated with rain and graupel, the reflectivity structure is less variable than the total hydrometeor structure, which also includes cloud water, cloud ice, and snow. Hence, retrievals of radar reflectivity profiles would be more certain than retrievals of either rain rate or total hydrometeor profiles.

The nonuniqueness between latent heating and T_B was illustrated by the example in Fig. 2a, which had an average structural difference of 140% at ΔT of 3 K. On average, the structural differences in AM_eL_i were somewhat less, with a value of about 90% at ΔT of 3 K. Similar values were found for the stratiform region. The larger uncertainty for the example in Fig. 2a is a result of taking profiles from other simulations. The average structural differences are greater than the magnitudes associated with profiles "1 and 2" and "1 and 3" in Fig. 3. Those comparisons are for the same vertical structure with one-half and one-fourth times the values in profile 1. Hence, the magnitude of the structural differences in latent heating profiles as a function of ΔT suggests that the profiles likely have their maxima at different altitudes.

3) IMPACT OF DIFFERENT MODEL MICROPHYSICS

To test whether the impact of the different microphysical schemes exceeded the inherent variability in T_B–cloud property relations, comparisons were made among the four microphysical schemes using AM_eL_i as the reference set of profiles. For each profile in AM_eL_i, the differences between that profile and all other profiles in AM_eL_i, BM_eL_i, AM_eH_i, and BM_eH_i were computed and sorted by the magnitude of the change in the brightness temperature vector.

Results for the hydrometeor structure, surface rain rate, and latent heating profiles are shown in Fig. 5. Here we made use of the entire convective region, defined as convective clouds with surface rain rate in excess of 1 mm h^{-1}, and the entire stratiform region, defined as stratiform clouds with surface rain rate in excess of 0.1 mm h^{-1}, to capture differences associated with developing convective cells and weaker precipitation regions.

(i) Structural differences

The impacts of model microphysical parameterizations are evident in comparing the average structural difference in hydrometeor profile as a function of ΔT (Figs. 5a,d) for the high-ice and low-ice runs. In scheme A, the variability in T_B–hydrometeor relations did not depend on the initial number of ice crystals assumed to be activated at 0°C. In contrast, scheme B was very sensitive to the NCIO parameter. The marked separation between BM_eL_i and BM_eH_i simulations demonstrates that the impact of microphysical settings on retrievals of cloud properties from passive microwave observations depends significantly on the details of the particular parameterization scheme used in the model. The variation between the low-ice and high-ice versions of scheme B was roughly 2 times the variability inherent in the T_B–hydrometeor relations for scheme A. Even when the two microphysical parameterizations have been tuned, as in the AM_eL_i and BM_eL_i simulations (Hristova-Veleva 2000), philosophical choices made in parameterization schemes can lead to significant additional uncertainty in T_B–cloud property relations for hydrometeor structure. These choices affected both the convective and the stratiform T_B–hydrometeor relations.

(ii) Surface rain rate

The impact of model microphysical parameterizations on surface rain rate–T_B relations (Figs. 5b,e) was considerably less than the impact on overall hydrometeor structure. Except for stratiform regions with small changes in ΔT, the additional variability associated with the different microphysical schemes was only a small fraction of the inherent variability associated with surface rain rate–T_B relations. The correlation between T_B at TMI frequencies and rain is strong enough to limit the impact of model microphysics on the retrieval of surface rain rate.

(iii) Latent heating

The overarching goal of TRMM is to determine the four-dimensional distribution of latent heating across the Tropics for input to climate models (Simpson et al. 1988). An unfortunate fact is that the variability in T_B–latent heating relations associated with different microphysical schemes is nearly as large as the inherent uncertainty in T_B–latent heating relations (Figs. 5c,f). This is true even though the two schemes are based on the

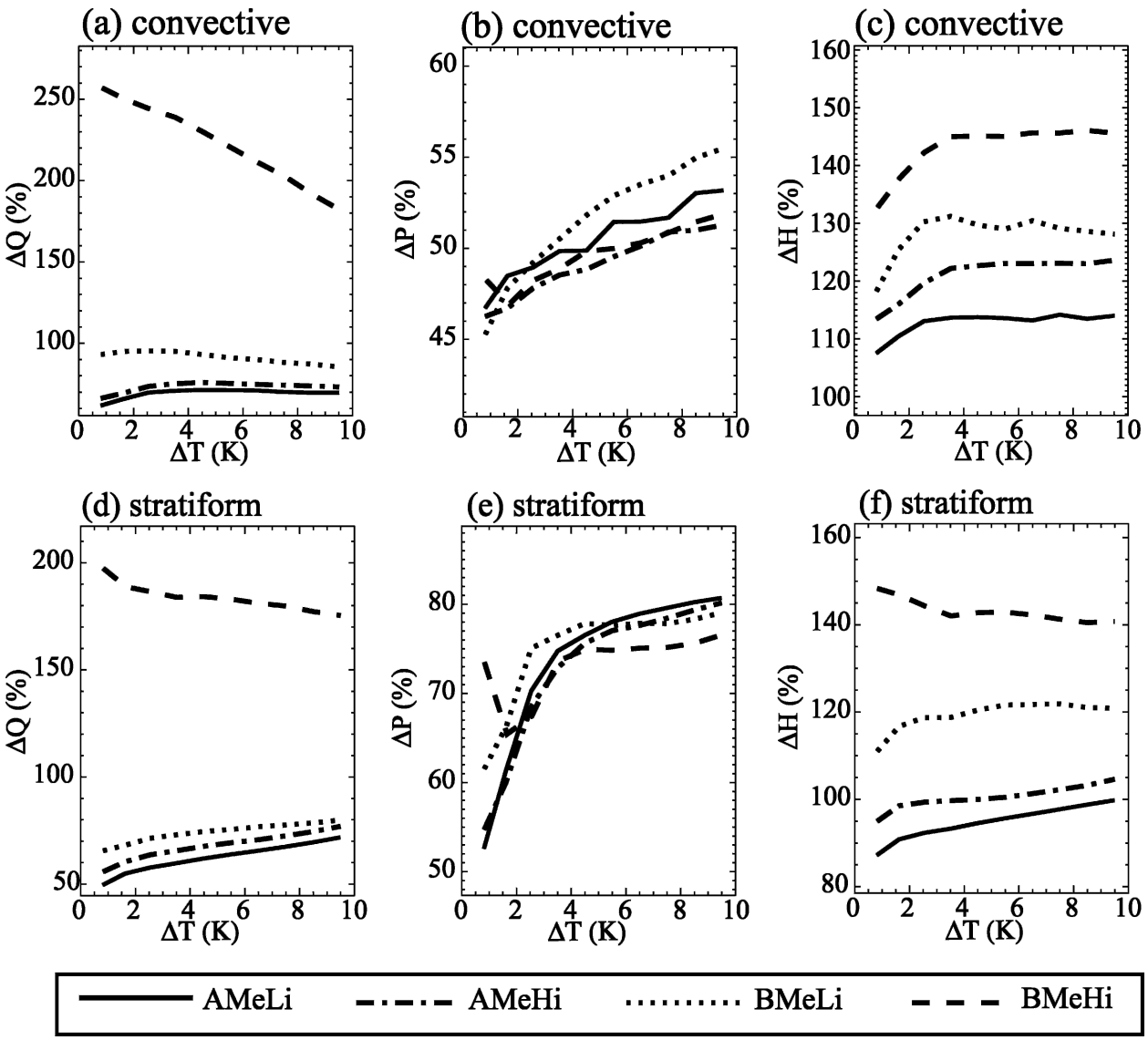

FIG. 5. Structural differences of (a) hydrometeor profiles, (b) surface precipitation rates, and (c) latent heating profiles for surface precipitation rates greater than 1 mm h^{-1} in convective clouds and (d) hydrometeor profiles, (e) surface precipitation rates, and (f) latent heating profiles for surface precipitation rates greater than 0.1 mm h^{-1} in stratiform clouds. Solid, dotted, dashed, and dot–dashed lines represent AM_eL_i, BM_eL_i, BM_eH_i, and AM_eH_i, respectively.

same bulk three-class ice/two-class water paradigm. Once again, scheme B showed the greatest range in variability. This result was due to the difference in the production of cloud ice, which affected both the hydrometeor structure as well as the vertical distribution of latent heating.

5. Effect of resolution on variability in T_B–cloud property relations

So far, the analyses presented have been conducted at high resolution, which allows for physical interpretation of the results relative to the dynamics and microphysics of individual cloud elements. Moreover, the high-resolution analyses can be applied to individual case studies based on data from airborne instruments like the Advanced Microwave Precipitation Radiometer (AMPR; Spencer et al. 1994). However, TRMM is a satellite mission. The relative importance of model microphysical parameterizations may depend on the scale at which the brightness temperatures are measured.

To examine the effect of resolution on the relationship between brightness temperature vectors and cloud

TABLE 2. Structural differences in hydrometeor, radar reflectivity, and latent heating profiles and difference in surface precipitation rates in percent over high and low resolutions in terms of ΔT in the range of 0 and 10 K in AM_eL_i. Regular and italic fonts represent high and low resolutions, respectively.

Structural difference	≥1 mm h^{-1} (convective)		≥0.1 mm h^{-1} (stratiform)	
Hydrometeor profile	50–70	*30–50*	40–75	*35–55*
Radar reflectivity profile	35–45	*23–30*	18–31	*15–23*
Latent heating profile	105–115	*65–90*	90–100	*75–85*
Surface precipitation rate	45–58	*32–47*	50–80	*35–70*

properties, all T_B in the AM_eL_i simulation were convolved over TMI footprint sizes using TMI antenna gain functions. All corresponding cloud properties were averaged over a 18×18 km^2 area, which approximates the middle of the TMI resolutions at the different frequencies.

As the resolution decreased, the variability between brightness temperatures and cloud properties also decreased for all of the parameters examined (Table 2). This result indicates that cloud properties at TMI scales do not have variability as large as that of individual profiles at high resolution. Structural differences in hydrometeor profiles decreased by roughly one-third of the amount found at high resolution for both convective and stratiform regions. The same was true for differences in the reflectivity profile. The variability, and hence uncertainty, in surface rain rate was reduced by about 12% over both convective and stratiform regions. On the other hand, variability in T_B–latent heating relations was reduced more in the convective region (30%) than in the stratiform region (15%). This result can be attributed to fundamentally more uniform vertical motions in stratiform regions.

The above results are somewhat contrary to those of Smith et al. (1994) who showed that rain retrievals are not significantly affected by resolution degradation. Factors that contribute to the discrepancy in the findings between this study and their study are that 1) this study used a large dataset from a numerical simulation and their study was confined to a limited set of observed brightness temperatures from AMPR and 2) this study treated the effect of convective and stratiform clouds separately, whereas the Smith et al. (1994) study did not distinguish between cloud types.

The reduction in variability noted in Table 2 indicates the degree to which spatial averaging can reduce the randomness of the T_B–cloud property relations that were illustrated in Fig. 2. In contrast, the variability in T_B–cloud property relations associated with the different microphysical parameterizations illustrated in Fig. 5 is not random. They represent a bias associated with

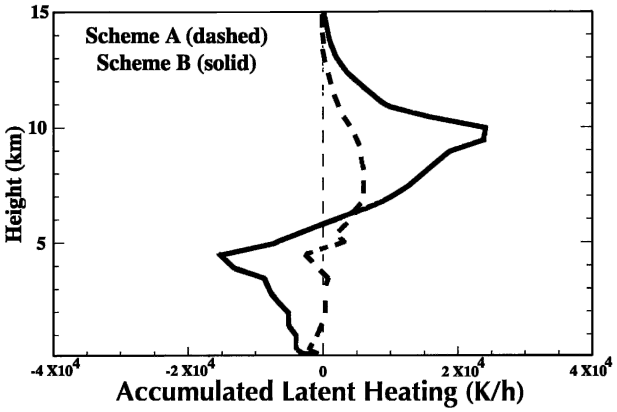

FIG. 6. Total accumulated latent heating (K h^{-1}) retrieved from TMI observations over Kwajalein during August 1999 for a simulation using scheme-A microphysical parameterizations (dashed line) and scheme-B microphysical parameterization (solid line).

systematic differences in the treatment of microphysical processes that lead to fundamentally different cloud structures and latent heating profiles (Part I). In that regard, spatial averaging increases the relative importance of model microphysics when compared with the inherent variability in T_B–cloud property relations.

To illustrate this, retrievals of latent heating were conducted over the Kwajalein, Republic of the Marshall Islands, region for August of 1999 (Fig. 6). The Collaborative Model for Multiscale Atmospheric Simulation (COMMAS; Skamarock and Klemp 1993) database used for this retrieval consisted of two simulations, both of which were high ice; one used the scheme-A microphysical parameterizations and the other used scheme B, initialized with a sounding from Trier et al. (1996) for a tropical oceanic squall line observed over the Pacific Ocean warm pool. Additional details are found in Seo (2000). The model brightness temperature calculations took into account the TRMM antenna gain function, and the cloud properties were averaged at an intermediate scale, that of the 37-GHz TMI footprint. The model database was partitioned into convective, stratiform, or mixed-mode footprints. Observed TMI data were classified according to Hong et al. (1999) and were used to retrieve EOF coefficients of the latent heating profile from the appropriate part of the database. The EOFs were used to reconstruct instantaneous footprint average latent heating profiles and were added to the sum shown in Fig. 6.

This result, while limited in scope, clearly shows that averaging enhanced the bias associated with the different microphysical schemes. The altitude of the maximum heating is shifted upward by ~2 km in scheme B relative to scheme A. Moreover, scheme B shows pronounced mid- to low-level cooling whereas

scheme A has almost no net heating or cooling in the lowest 4 km.

6. Implications for retrieved latent heating

The EOF framework used in this study provides one method for quantifying the uncertainty in retrieving cloud properties using passive microwave observations at TMI frequencies. It should be understood that this approach retrieves the perturbation from the mean profile. Large uncertainties in retrieving the EOF coefficient indicate that the profile cannot be adjusted reliably from the mean structure associated with the model database.

a. Stratiform regions

For stratiform region latent heating, for which the uncertainty in retrieving the EOF coefficient is large, it may be best to use other methods to estimate latent heating. For example, the convective–stratiform heating algorithm developed by Tao et al. (1993) assumes that the shape of stratiform heating is the mean over the stratiform area in the cloud model. Their approach adjusts the magnitude, but not the structure, of the heating according to the precipitation rate. This adjustment approach implies that the model database has the correct mean heating profile. A similar assumption is made in Shige et al. (2004). A key aspect of their approach is to partition the database according to echo top, so that shallow convection can be separated from deep convection, or by the precipitation rate at the melting level as in the case of deep stratiform cloud. Then all of the heating profiles for increments in echo top for convective clouds, or melting level precipitation rate for deep stratiform clouds, are averaged. Using a radar profile as input, they retrieve the mean heating for that echo top or melting-level precipitation rate. In their method, each cloud profile that has the same echo top or same melting-level precipitation rate will have the same heating profile, regardless of the vertical structure of the hydrometeors. Again, the assumption is that the model has produced the correct mean profile.

Given the current limitations in bulk three-class ice model microphysical parameterizations and the difficulty in simulating broad regions of stratiform clouds dominated by snow instead of graupel, it is not clear that model databases have accurate mean stratiform heating structures. This is true for the current study as well. Moreover, we note that different implementations of bulk three-class ice microphysical parameterizations can produce differences in the mean structure of the stratiform region latent heating, even with the same microphysical settings (Part I).

Nevertheless, given the common weaknesses in retrieval databases, adjusting the model means using the techniques of Tao et al. (1993) or Shige et al. (2004) is likely more appropriate than using the EOF coefficient to adjust the model mean. This might change if additional information relevant to snow and cloud ice, like higher-frequency brightness temperatures or cloud radar, were used in the retrieval.

b. Convective regions

In convective regions, for which departures from the mean can be substantial, an inability to retrieve the perturbation associated with a given set of brightness temperature observations would lead to large errors in retrieved cloud structure. The analysis suggests that there fortunately is skill in retrieving the EOF coefficient for convective-region latent heating, especially when all of the TMI frequencies are used. Analyses conducted for 36×36 km^2 and 72×72 km^2 footprints (not shown) indicate that the uncertainty in retrieving the EOF coefficient for latent heating is about 30%–40%, which is slightly better than the 50% found at high resolution. Averaging over time and space may further reduce random errors.

Hence, EOF-based methods are more useful over convective regions than over stratiform regions. With its ability to account for variation in the vertical structure of latent heating, the EOF technique may be more appropriate over convective areas than are methods that adjust the magnitude of the model mean or assume that clouds with the same echo top will have the same heating profile. Regardless, the retrieval of latent heating is intimately tied to the microphysical parameterizations used in the cloud models that generated the retrieval database. Although scheme A exhibited less sensitivity to the microphysical parameters tested here, it is unclear as to whether this behavior should be viewed as a strength or as a weakness in the model. It may be a matter of philosophical preference as to whether or not a microphysical scheme should be sensitive or invariant to physical factors that are poorly known but physically meaningful, like the initial number of ice crystals assumed to be activated at 0°C. It may also be difficult to justify implementing more sophisticated microphysical schemes when observational guidance needed to validate their performance is unavailable.

7. Conclusions

The impact of model microphysics on the retrieval of cloud properties based on passive microwave observations was examined using a three-dimensional, nonhy-

drostatic, adaptive-grid cloud model to simulate a mesoscale convective system over ocean. Two different microphysical schemes that are both based on a bulk two-class liquid and three-class ice parameterization were tested by adjusting the assumed number of ice crystals activated at 0°C (the so-called NCIO parameter). The low-NCIO runs, representative of a midlatitude environment with large concentrations of cloud condensation nuclei (CCN), allowed supercooled cloud water to accumulate. High-NCIO runs ensured that enough cloud ice was present to absorb excess water vapor and minimize the accumulation of supercooled cloud water, representative of convection over the tropical oceans and the Amazon.

The uncertainty in retrieved cloud properties was quantitatively determined using an empirical orthogonal function (EOF) framework. For convective surface rain rates, the uncertainty varied between 20% and 60% depending on which combination of passive and active microwave observations was used in the retrieval. The uncertainty in surface rain rate did not depend on the microphysical scheme or the parameter settings except for retrievals over stratiform regions based on 85-GHz T_B by itself, or 85-GHz T_B and radar reflectivity combined. The different behavior for convective and stratiform regions was attributed to the influence of snow on stratiform rain and the relatively low correlations between EOFs of snow and microwave brightness temperatures at TMI frequencies (Part I).

Systematic differences in the treatment of the production of cloud water, cloud ice, and snow between the two parameterization schemes led to significant differences in the uncertainty in retrievals of those cloud properties. Scheme A, based on Tao and Simpson (1993), produced cloud structures that were somewhat layered, where high concentrations of cloud ice and snow were also associated with high concentrations of graupel and rain. In contrast, scheme B, based on Keenan et al. (1994), produced cloud structures with a more uniform distribution of cloud ice and snow (Hristova-Veleva 2000). Because the TMI frequencies respond well to rain and graupel, scheme A exhibited less uncertainty in retrievals of snow and cloud ice than did scheme B. Moreover, scheme A, in which excessive water vapor is partitioned into cloud water and cloud ice somewhat independently of the number of ice crystals present, showed less sensitivity to the NCIO parameter than did scheme B.

To determine whether the variation associated with the different microphysical parameterizations was significant, a comparison was made with the inherent variability in T_B–cloud property relations. The inherent variability in T_B–cloud property relations also provides insight to the level of uncertainty in Bayesian retrieval methods (Evans et al. 1995; Olson et al. 1999) in which a model database is searched to find profiles that closely match an input brightness temperature vector. It was found that small changes in the input T_B vector used to drive the retrieval could lead to significant differences in the vertical structure of retrieved cloud properties, especially those properties that are poorly correlated with TMI channels. Even within the same simulation there existed large variability in hydrometeor structure and latent heating profiles for relatively small changes in the T_B vector. Indeed, the variation in latent heating was greater than what would be expected from a mere difference in the magnitudes of the profiles, suggesting that the vertical profiles had different altitudes for the peak heating and cooling. There is a fundamental lack of correlation between instantaneously measured T_B and latent heat release. In physical terms, the latent heat release might be better correlated with a change of T_B in time than with an instantaneously measured T_B.

When the variability among the four simulations was plotted in terms of departures from a reference database (the low-NCIO version of scheme A), it was found that differences in the microphysical parameterizations could double the uncertainty in hydrometeor structure and increase the variability in latent heating by about 50%. Nearly all of the increase was associated with the range of variability among the scheme-B simulations. Thus, depending on which microphysical parameterization is used in the model, the impact of model microphysics on retrieved hydrometeor and latent heating structure can exceed the inherent uncertainty associated with nonuniqueness in T_B–cloud property relations.

This result does not imply that one scheme is better than the other. Instead, it suggests that retrievals of cloud properties from passive microwave observations are limited by the accuracy of microphysical parameterizations used in cloud-resolving models. This fundamental result is independent of whether the analysis is conducted at the resolution of the model output or at the scales of satellite footprints. Averaging over TRMM footprints reduced the inherent variability associated with randomness in T_B–cloud property relations. However, the systematic differences associated with the model microphysics represent a bias. In that regard, spatial averaging increases the relative importance of model microphysics when compared with the inherent variability in T_B–cloud property relations.

Acknowledgments. This research was supported by the National Aeronautics and Space Administration

(NASA) Tropical Rainfall Measuring Mission (TRMM) under Grants NAG5-9697 and NAG5-13262. The authors thank Dr. K.-Y. Kim for valuable advice in examining uncertainties in the retrievals. TRMM data were provided by the Goddard Distributed Active Archive Center.

REFERENCES

Adler, R. F., H.-Y. M. Yeh, N. Pasad, W.-K. Tao, and J. Simpson, 1991: Microwave simulations of a tropical rainfall system with a three-dimensional cloud model. *J. Appl. Meteor.,* **30,** 924–953.

Biggerstaff, M. I., and S. A. Listemaa, 2000: An improved scheme for convective/stratiform echo classification using radar reflectivity. *J. Appl. Meteor.,* **39,** 2129–2150.

——, E.-K. Seo, S. Hristova-Veleva, and K.-Y. Kim, 2006: Impact of cloud model microphysics on passive microwave retrievals of cloud properties. Part I: Model comparison using EOF analyses. *J. Appl. Meteor. Climatol.,* **45,** 930–954.

DeMaria, M., 1985: Linear response of a stratified tropical atmosphere to convective forcing. *J. Atmos. Sci.,* **42,** 1944–1959.

Evans, K. F., J. Turk, T. Wong, and G. L. Stephens, 1995: A Bayesian approach to microwave precipitation profile retrieval. *J. Appl. Meteor.,* **34,** 260–279.

Hartmann, D. L., H. H. Hendon, and R. A. Houze Jr., 1984: Some implications of the mesoscale circulations in tropical cloud clusters of large-scale dynamics and climate. *J. Atmos. Sci.,* **41,** 113–121.

Heymsfield, G. M., and R. Fulton, 1988: Comparison of high-altitude remote aircraft measurements with the radar structure of an Oklahoma thunderstorm: Implications for precipitation estimation from space. *Mon. Wea. Rev.,* **116,** 1157–1174.

Hong, Y., C. D. Kummerow, and W. S. Olson, 1999: Separation of convective and stratiform precipitation using microwave brightness temperature. *J. Appl. Meteor.,* **38,** 1195–1213.

Houze, R. A., Jr., 1982: Cloud clusters and large-scale vertical motions in the tropics. *J. Meteor. Soc. Japan,* **60,** 396–409.

Hristova-Veleva, S. M., 2000: Impact of microphysical parameterizations on simulated storm evolution and remotely-sensed characteristics. Ph.D. dissertation, Texas A&M University, 201 pp.

Johnson, D. E., 1984: Partitioning tropical heat and moisture budgets into cumulus and mesoscale components: Implications for cumulus parameterization. *Mon. Wea. Rev.,* **112,** 1590–1601.

Keenan, T. D., B. Ferrier, and J. Simpson, 1994: Development of structure of a maritime continent thunderstorm. *Meteor. Atmos. Phys.,* **53,** 185–222.

Kummerow, C., 1993: On the accuracy of the Eddington approximation for radiative transfer in the microwave frequencies. *J. Geophys. Res.,* **98,** 2757–2765.

——, and L. Giglio, 1994: A passive microwave technique for estimating rainfall and vertical structure information from space. Part I: Algorithm description. *J. Appl. Meteor.,* **33,** 3–18.

——, I. M. Hakkarinen, H. F. Pierce, and J. A. Weinman, 1991: Determination of precipitation profiles from airborne passive microwave radiometric measurements. *J. Atmos. Oceanic Technol.,* **8,** 148–158.

——, W. S. Olson, and L. Giglo, 1996: A simplified scheme for obtaining precipitation and vertical hydrometeor profiles from passive microwave sensors. *IEEE Trans. Geosci. Remote Sens.,* **34,** 1213–1232.

——, W. Barnes, T. Kozo, J. Shiute, and J. Simpson, 1998: The Tropical Rainfall Measuring Mission (TRMM) sensor package. *J. Atmos. Oceanic Technol.,* **15,** 809–817.

——, and Coauthors, 2000: The status of the Tropical Rainfall Measuring Mission (TRMM) after two years in orbit. *J. Appl. Meteor.,* **39,** 1965–1982.

Leary, C. A., and R. A. Houze Jr., 1979: The structure and evolution of convection in a tropical cloud cluster. *J. Atmos. Sci.,* **36,** 437–457.

Lin, Y.-L., R. D. Farley, and H. D. Orville, 1983: Bulk parameterization of the snow field in a cloud model. *J. Climate Appl. Meteor.,* **22,** 1065–1092.

Malkus, J. S., 1962: Large-scale interactions. *The Sea—Ideas and Observations on Progress in the Study of the Seas, Vol. 1: Physical Oceanography,* M. N. Hill, Ed., Interscience, 88–294.

Neter, J., M. H. Kutner, C. J. Nachtsheim, and W. Wasserman, 1996: *Applied Linear Statistical Models*. 4th ed. Irwin Press, 1408 pp.

Olson, W. S., C. D. Kummerow, G. M. Heymsfield, and L. Giglio, 1996: A method for combined passive–active microwave retrievals of cloud and precipitation profiles. *J. Appl. Meteor.,* **35,** 1763–1789.

——, ——, Y. Hong, and W.-K. Tao, 1999: Atmospheric latent heating distributions in the Tropics derived from satellite passive microwave radiometer measurements. *J. Appl. Meteor.,* **38,** 633–664.

Panegrossi, G., and Coauthors, 1998: Use of cloud model microphysics for passive microwave-based precipitation retrieval: Significance of consistency between model and measurement manifolds. *J. Atmos. Sci.,* **55,** 1644–1673.

Riehl, H., and J. S. Malkus, 1958: On the heat balance in the equatorial trough zone. *Geophysica,* **6,** 503–538.

——, and J. Simpson, 1979: The heat balance of the equatorial trough zone, revisited. *Contrib. Atmos. Phys.,* **52,** 287–304.

Rutledge, S. A., and P. V. Hobbs, 1984: The mesoscale and microscale structure and organization of clouds and precipitation in midlatitude clouds. Part XII: A diagnostic modeling study of precipitation development in narrow cold frontal rainbands. *J. Atmos. Sci.,* **41,** 2949–2972.

——, and R. A. Houze Jr., 1987: A diagnostic modeling study of the trailing-stratiform region of a midlatitude squall line. *J. Atmos. Sci.,* **44,** 2640–2656.

Seo, E.-K., 2000: Sensitivity of hydrometeor profiles and satellite brightness temperatures to model microphysics from MCSs over land and ocean: Model comparison using EOF analysis and implications for rain and latent heat retrievals. Ph.D. dissertation, Texas A & M University, 177 pp.

Shige, S., Y. N. Takayabu, W.-K. Tao, and D. E. Johnson, 2004: Spectral retrieval of latent heating profiles from TRMM PR data. Part I: Development of a model-based algorithm. *J. Appl. Meteor.,* **43,** 1095–1113.

Simpson, J., R. F. Alder, and G. R. North, 1988: A proposed Tropical Rainfall Measuring Mission (TRMM) satellite. *Bull. Amer. Meteor. Soc.,* **69,** 278–295.

Skamarock, W. C., and J. B. Klemp, 1993: Adaptive grid refinement for two-dimensional and three-dimensional nonhydrostatic atmospheric flow. *Mon. Wea. Rev.,* **121,** 788–804.

Smith, E. A., A. Mugnai, H. J. Cooper, G. J. Tripoli, and X. Xiang, 1992: Foundations for statistical-physical precipitation retrieval from passive microwave satellite measurements.

Part I: Brightness temperature properties of a time-dependent cloud-radiation model. *J. Appl. Meteor.,* **31,** 506–531.

——, X. Xiang, A. Mugnai, and G. J. Tripoli, 1994: Design of inversion-based precipitation profile retrieved algorithm using an explicit cloud model for initial guess microphysics. *Meteor. Atmos. Phys.,* **54,** 53–78.

Spencer, R. W., R. E. Hood, F. J. LaFontaine, E. A. Smith, J. Galliano, and E. Lobl, 1994: High-resolution imaging of rain systems with the Advanced Microwave Precipitation Radiometer. *J. Atmos. Oceanic Technol.,* **11,** 849–857.

Stith, J. L., J. E. Dye, A. Bansemer, and A. J. Heymsfield, 2002: Microphysical observations of tropical clouds. *J. Appl. Meteor.,* **41,** 97–117.

Tao, W.-K., and J. Simpson, 1993: Goddard Cumulus Ensemble Model. Part I: Model description. *Terr. Atmos. Oceanic Sci.,* **4,** 35–72.

——, ——, S. Lang, M. McCumber, R. Adler, and R. Penc, 1990: An algorithm to estimate the heating budget from vertical hydrometeor profiles. *J. Appl. Meteor.,* **29,** 1232–1244.

——, S. Lang, J. Simpson, and R. Adler, 1993: Retrieval algorithms for estimating the vertical profiles of latent heat release: Their application for TRMM. *J. Meteor. Soc. Japan,* **71,** 685–700.

Trier, S. B., W. C. Skamarock, M. A. LeMone, D. B. Parsons, and D. P. Jorgensen, 1996: Structure and evolution of the 22 February 1993 TOGA COARE squall line: Numerical simulations. *J. Atmos. Sci.,* **53,** 2861–2886.

Weinman, J. A., and R. Davies, 1978: Thermal microwave radiances from horizontally finite clouds of hydrometeors. *J. Geophys. Res.,* **83,** 3099–3107.

Willis, P. T., and A. J. Heymsfield, 1989: Structure of the melting layer in mesoscale convective system stratiform precipitation. *J. Atmos. Sci.,* **46,** 2008–2025.

Yanai, M., S. Esbensen, and J.-H. Chu, 1973: Determination of bulk properties of tropical cloud clusters from large-scale heat and moisture budgets. *J. Atmos. Sci.,* **30,** 611–627.